Draft version August 30, 2021
Typeset using LaTeX **twocolumn** style in AASTeX631

Star Formation in Bright-Rimmed Cloud SFO 14

Claire Finley[1,2] and Larry Morgan[1]

[1] *Green Bank Observatory*
155 Observatory Rd.
Green Bank, WV 24944, USA
[2] *Villanova University*
800 E Lancaster Ave.
Villanova, PA 19085, USA

ABSTRACT

Using ^{12}CO, ^{13}CO, and C^{18}O data from the James Clerk Maxwell Telescope, ammonia data from the Green Bank Telescope, and archival radio data from the NRAO/VLA Sky Survey we examined the possibility of triggered star formation in bright-rimmed cloud SFO 14 to build a complete picture of the cloud and its layers. Python commands were used to create parameter maps for the CO data, and maps of integrated intensity, spectral line velocity, line width, optical depth, excitation temperature, and turbulent velocity dispersion were derived. An analysis of these parameter maps in conjunction with the ammonia parameter maps and radio contours indicates trends in the cloud that are consistent with triggering predictions; however, the evidence is not quantitative enough to conclude that triggering is clearly present.

Keywords: HII region, star formation, bright-rimmed clouds, ionized boundary layer

Contents

1. INTRODUCTION

Bright-rimmed clouds (hereafter, BRCs) are a class of molecular cloud with optically bright rims that sit at the edge of ionized 'bubbles' created by a nearby massive star. The massive star propagates out radiation, which ionizes surrounding material. This ionized bubble then expands until its ionizing photon flux matches that of the recombination of atomic or molecular material, which outlines the edge of the bubble. This edge-defining occurs rapidly with a slower expansion pushing material away from the star. The movement of the material away from the star causes its surrounding HII region to expand. When the HII region expands into a nearby molecular cloud, it tends to push away low-density gas faster than high-density gas (Bertoldi 1989). This creates an optically-bright rim, which is the reason why the cloud is classified as a BRC. The semi-stable boundary between the ionizing bubble and the BRC is known as the ionized boundary layer (hereafter, IBL). Between the IBL and the cloud itself is a recombination layer known as the photodissociation region (hereafter, PDR), and the center of the cloud is a core where often a new HII region is forming. The core, especially in the case of SFO 14 (discussed in further detail below) is best observed through optically thin molecules such as ^{13}CO or C^{18}O (Morgan et al. 2008).

BRCs are often the site of young protostellar cores; thus, they host star formation. Previous papers theorize that stars may have been induced or triggered to form inside BRCs when ionization-induced shocks from the nearby massive star propagate through the cloud (Bertoldi 1989). This process is known as radiation-driven implosion (Bertoldi 1989).

BRCs have been qualitatively and quantitatively examined, with many studies covering wavelengths from low-frequency radio (Morgan et al. 2008) to optical (Sugitani et al. 1991) or X-ray emission. A widely-studied group of BRCs come from the list discerned by Sugitani, Fukui, and Ogura, known as the SFO catalogue (Sugitani et al. 1991). However, not all the BRCs in the SFO catalogue are good candidates for triggered

star formation. A 2009 study by Morgan et al. found that the surface temperature was significantly higher for clouds where triggering was likely, and a number of BRCs in the catalogue were thus determined to be unlikely candidates for photoionized triggering. A subsequent 2010 study by Morgan et al. found that the likely-triggered clouds had significantly higher turbulent velocity dispersions than clouds unlikely to be subject to this form of triggering. The combination of these two papers reduced the list of SFO objects where triggering was likely.

While there are a number of potentially-triggered BRCs in the SFO catalogue for which there exists sufficient data, it was determined that the analysis process could be streamlined by focusing on only one BRC first. This paper investigates SFO 14, also known as IC 1848. SFO 14 has been previously investigated as a good candidate for triggering because of its compact HII region and molecular outflows that indicate star formation (Morgan et al. 2004). Cross-referencing this analysis with literature proves that it has a young embedded cluster containing massive stars, and triggering is likely (Morgan et al. 2004). The data analysis performed for SFO 14 in this paper can be repeated for the rest of the BRCs where triggering is likely.

This paper focuses on CO and ammonia data for SFO 14. The CO data includes the J=3→2 transitions for ^{12}CO, ^{13}CO, and C^{18}O. The data was taken using the James Clerk Maxwell Telescope (JCMT), and the molecules have rest frequencies of 345.8 GHz, 330.6 GHz, and 329.3 GHz respectively. The JCMT has a beam resolution of 14.6". It is important to note that ^{12}CO is optically thick and ^{13}CO and C^{18}O are optically thin. The ammonia data was taken with the Green Bank Telescope with a beam resolution of about 30", and has a rest frequency of 23.69 GHz for the (1,1) transition and 23.72 GHz for the (2,2) transition. It is useful to study these molecules because they map different parts of the cloud. Since ^{12}CO is optically thick, it is generally best suited for tracing the surface layers of the cloud. C^{18}O emission, being optically thin, better traces the dense core embedded within the cloud. Ammonia, which is moderately optically thick, falls between the two extremes of optically thin and thick and reveals the broader molecular cloud environment, which may potentially link the outer layers of the molecular cloud to the inner core.

It is important to compare as many different data sets as possible to build the best picture of the cloud. So, to compare with both the ammonia and CO data, archival radio data is taken from the NRAO/VLA Sky Survey to cover more wavelengths (Morgan et al. 2004). Radio wavelengths are particularly useful for modeling the IBL of BRCs as these trace the free-free emission associated with ionized material.

The primary goal of this paper is to investigate the possibility of triggering through an analysis of the emission from the different molecules found in and around BRCs. A secondary goal is to develop a more complete picture of BRCs' behavior and structure by making a model of the cloud's layers. It is hoped that this model will apply to other clouds besides SFO 14.

2. PROCEDURE

In order to build a comprehensive understanding of SFO 14, we needed to examine a multitude of different combinations of molecular maps.

Reduced spectral cubes already existed for both the ammonia and CO data. The ammonia data had incorrect FITS headers, which were rectified by creating a Python script that edited 'CDELT1' and 'CDELT2' parameters in the header. In order to view these cubes, a Python script was written using the spectral_cube package, a part of the astropy module.

Next, moment maps were created, where the zeroth moment represents the integrated intensity of the spectral line (**Fig. 1**), the first moment represents the velocity of the spectral line (**Fig. 2**), and the second moment represents the velocity dispersion of the spectral line (**Fig. 3**). Line width maps were also created using the full width at half maximum of the spectral line (**Fig. 4**). First, the units of the third dimension of each map were converted from spectral channels to radio velocity in km/s. Then, using the moment attribute of the spectral_cube package, the maps were created and saved as FITS files.

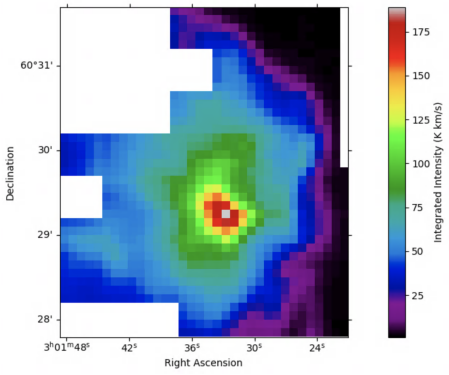

Figure 1. Moment 0 map for ^{12}CO

Then, the max attribute of the spectral_cube package was used to create two-dimensional maps of the peak

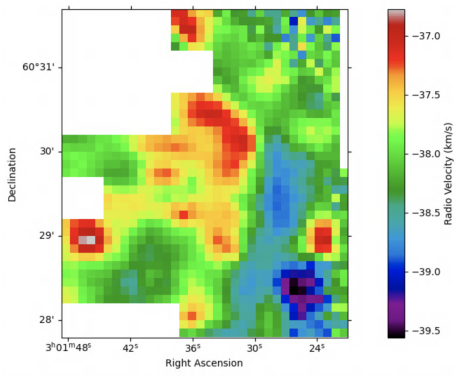

Figure 2. Moment 1 map for ^{12}CO

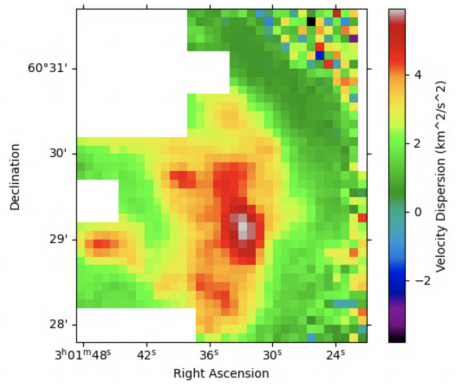

Figure 3. Moment 2 map for ^{12}CO

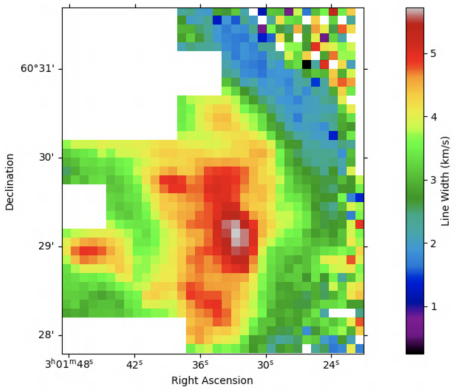

Figure 4. Line Width map for ^{12}CO

emission in terms of antenna temperature for each respective molecule. An example is shown in **Fig. 5**

Equations for opacity/optical depth, excitation temperature, and column density were then derived from Planck's Law ($B_\nu = \frac{2h\nu^3}{c^2}\frac{1}{e^{\frac{h\nu}{k_B T}}-1}$) using a method analogous to that of Morgan et al. 2009. Assumptions were made that the cloud appears as a blackbody if it is in thermal equilibrium and the Rayleigh approximation holds true that hν << k_BT, where h is Planck's constant, ν is the radiation frequency, k_B is Boltzmann's constant, and T is the thermodynamic temperature of the cloud. It should be noted that any temperature we measure is the sum of the cosmic microwave background (CMB) temperature and the object's brightness temperature, and the CMB temperature is removed through the calibration process. Through a number of substitutions, the equation for optical depth is arrived at:

$\frac{T_x}{T_y} = \frac{1-e^{-\tau_x}}{1-e^{-\tau_y}}$

Opacity is represented by τ, and an opacity map (**Fig. 6**) shows the amount of material in a given pixel. In order to calculate τ, we wrote a script containing an array of possible values with boundary values at the respective extremes of likelihood, counting in very small increments between these two values. The script then ran through each value in the array, plugging guesses in for τ until it arrived on a value that satisfied the equation. This was possible assuming that the following equation is true for the ratio of the optical depth between two molecules at a given temperature: $\tau_x = \chi\tau_y$, where χ is the relative abundance. The assumed χ for the ^{12}CO/^{13}CO ratio is 60, for the ^{12}CO/C^{18}O ratio is 500, and for the ^{13}CO/C^{18}O ratio is 10. These values are not very precise, and further studies should be conducted to refine these values. In addition, this method was not used to compare the ^{12}CO and C^{18}O data as the difference in optical depth is too extreme. This method is most effective when the two molecules being compared are both optically thin.

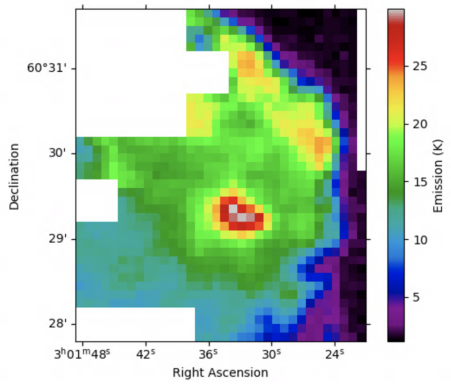

Figure 5. The ^{12}CO map at the point of maximum emission

Next, excitation temperature maps were produced. Excitation temperature describes the temperature at which two molecules will be at a constant proportionality, or the temperature of the cloud if it is in thermal equilibrium. The following equation describes the excitation temperature for a given molecule:

$T_{ex} = T_0\{ln(1 + \frac{T_0}{J(T_b)+(T_A^*)_x/\eta_b\Phi(1-e^{-\tau_x})})\}^{-1}$

Where $T_0 = \frac{h\nu}{k_B}$, $J(T_b) = T_0[e^{\frac{T_0}{T_b}} - 1]^{-1}$, T_b is the temperature of ambient background (taken as 2.7 K), T_A^* is corrected antenna temperature for given molecule, η_b is the beam efficiency, Φ is the beam filling factor, and optical depth τ was previously derived. Excitation temperature maps were produced by filling all the constants into this equation and then utilizing the previously-generated optical depth maps for τ and the maximum emission maps for T_A^*.

Last, turbulent velocity dispersion maps were produced. First, the mass of a CO molecule was converted to atomic mass units and saved as a variable. Then, the equation for thermal velocity dispersion was used to create an array of thermal velocity dispersion data, and is as follows:

$dVThermal = (\sqrt{8 * k_B * T_{ex} ln(2)/m})/1000$

Where k_B is the Boltzmann constant, T_{ex} is the excitation temperature map for the given molecule, and m is the mass of CO in atomic mass units (here, 4.64966e-26). Using the thermal velocity dispersion data, turbulent velocity maps can be derived, based on the equation:

$dvTurbulent = \sqrt{COdVdata^2 - dvThermal^2}$

Where COdVdata is the line width map for a given molecule with the infinite/nan values removed. We assume that the only contributions to the cloud's velocity dispersion are thermal and turbulent, since other factors are too small to make a noticeable contribution. Then, we assume line width/velocity dispersion is Gaussian. The sum of two independent normally distributed random variables is normal, with its variance being the sum of the two variances; in this case, $COdVdata^2 = dvThermal^2 + dvTurbulent^2$. So, to find the turbulent velocity dispersion, we subtract the square root of the thermal velocity dispersion from the total velocity dispersion.

3. ANALYSIS AND RESULTS

Each parameter map that was produced gives unique insights to the cloud and its behavior. The zeroth moment map (**Fig. 1**) shows the integrated intensity of the cloud's spectral line. Integrated intensity shows where material is gathered and its strength is correlated with both the concentration of that material along the line-of-sight and that material's thermodynamic temperature. In the zeroth moment maps we produced, we see a dense core and a few layers of diffuse gas surrounding it. The first moment describes the velocity of the spectral line. Looking at our maps (**Fig. 2**), the cloud is very homogeneous in velocity with an overall negative velocity, indicating that the cloud is moving towards the observer. The second moment (**Fig. 3**) and line width (**Fig. 4**) maps show a quiescent region of gas right at the surface of the cloud that might be an area of suppressed turbulent motion. In addition to this, the line width is smaller around the edge of the cloud, suggesting that the bulk velocity may be directed into the cloud, moving faster near the center. There is a very sharp boundary between the areas with smaller and larger line widths, which should be investigated in future studies to determine why the boundary might be so defined. The maximum emission map (**Fig. 5**) shows that same diffuse region being intensely heated, nearly as hot as the star-forming core of the cloud. This, coupled with the excitation temperature map for ^{12}CO (**Fig. 8**) suggests that there is an outside factor that is still heating up the cloud, even though the cloud likely formed a long time ago.

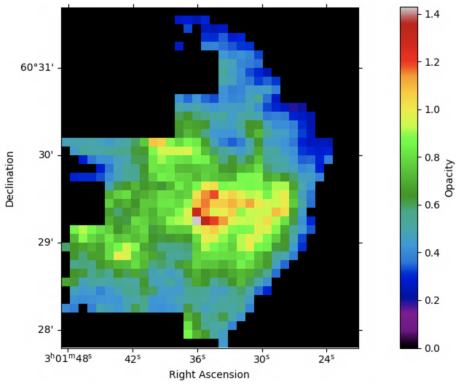

Figure 6. The ^{13}CO opacity map

The opacity map (**Fig. 6**) estimates a measure of molecular column density, often used as a proxy for volume density. In the ^{13}CO opacity map, there is a diffuse region tracing the entire exterior of the cloud and a denser pocket near the core. This is expected as opacity maps of optically thin molecules are expected to show the denser regions of where a molecule is, and ^{13}CO is an optically thin molecule so denser pockets of it should be found closer to the cloud's core.

Looking at the turbulent velocity dispersion for ^{12}CO (**Fig. 7**), there is a defined outline on the edge of the cloud that appears to encompass the same area that is intensely heated on the excitation temperature map. This is coincident with emission arising from the the IBL of the cloud (**Fig. 10**). The increased pressure of the IBL, along with the apparent heating exhibited by the excitation temperature map, might suggest a higher level of turbulent activity in this region. However, we see the opposite in **Fig. 7**, with a somewhat uniform region of fairly inert velocity dispersion in the top right of the cloud. This may be explained in several different ways, with potential suppression of the gas dynamical activity

in this region occurring due to the directional pressure of the IBL. Alternatively, this could be a simple line of sight effect due to the small depth of the path through the cloud at this edge region. In either case, it may also be possible that the bulk of the cloud is moving away from the IBL and toward the interior of the cloud. This could also manifest in an apparent diminishing of the turbulent velocity dispersion along the line of sight.

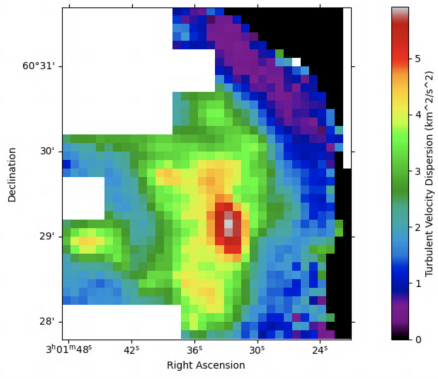

Figure 7. The ^{12}CO turbulent velocity dispersion map

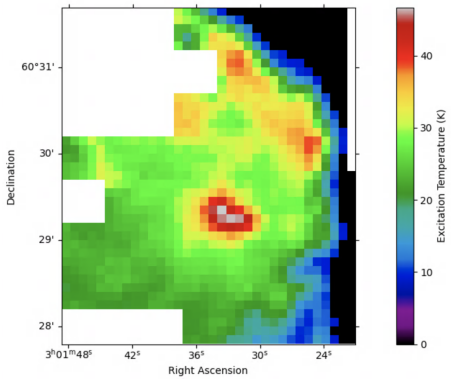

Figure 8. The ^{12}CO excitation temperature map

Similar to the opacity map, plotting the excitation temperatures for different tracers (**Fig. 8**) helps clearly map different density environments. So, seeing the gradient from the ^{12}CO heated at the surface and the ammonia heated only at the core is concurrent with predictions.

Cross-comparing between ammonia and CO data and radio contours, a pattern appears. The heated area in the ^{12}CO excitation temperature map (**Fig. 8**) matches up with the radio contours in white (**Fig. 9**), which show where the IBL is. The ammonia contours overlaid on the ^{12}CO excitation temperature map (**Fig. 10**) show matching outlines of the core and its location, which is hot and dense in both. The ammonia temperature map (**Fig. 9**) shows what appears to be diffuse material being blown away from the core in small pockets, or "bunny ears", as a predictive model by Lefloch & Lazareff 1994 (**Fig. 11**) terms them. This indicates pressure waves driving through the cloud from the IBL, forming what could be secondary and even tertiary areas of star formation. However, more investigation and analysis must be conducted to examine if higher-level star formation is occurring in these "bunny ears".

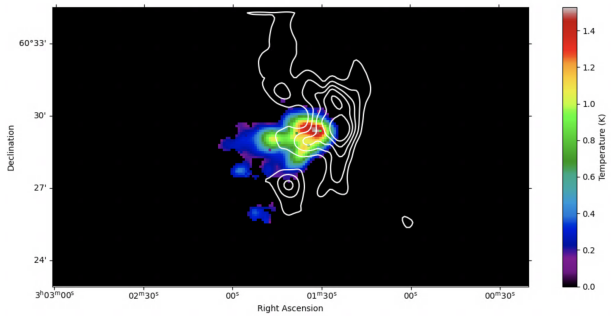

Figure 9. The ammonia temperature map with radio contours overlaid in white. The radio data outlines the cloud's IBL, and the ammonia data shows "bunny ears" like the Lefloch and Lazareff model predicts on the lower left edge of the cloud(**Fig. 10**).

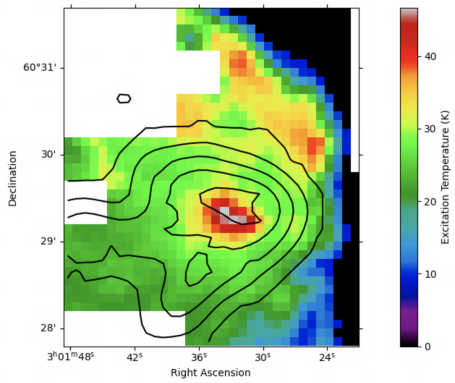

Figure 10. The ^{12}CO excitation temperature map with ammonia temperature map contours overlaid. The points of highest temperature nearly overlap, which indicates the location of the cloud's dense, hot core where new star formation is occurring.

4. DISCUSSION AND FUTURE OBSERVATIONS

Taking all of these insights into consideration, we can create a rough sketch for a model, containing four layers. The innermost layer and core of the BRC is very dense, hosts the newest star formation, and is forming a new HII region. Just outside the core, the second layer is a moderately dense envelope for the core. Surrounding that, layer three is a diffuse cloud that provides large-scale pressure; this layer is traced by the more widely-

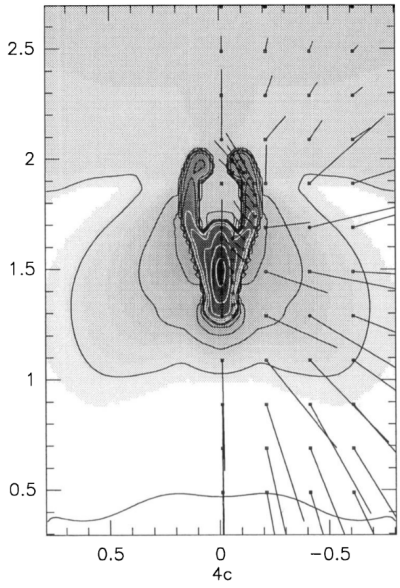

Figure 11. A model from Lefloch & Lazareff 1994 showing pressure propagating through the cloud and pushing material beyond the star-forming core to make new envelopes that could possibly host secondary or tertiary star formation.

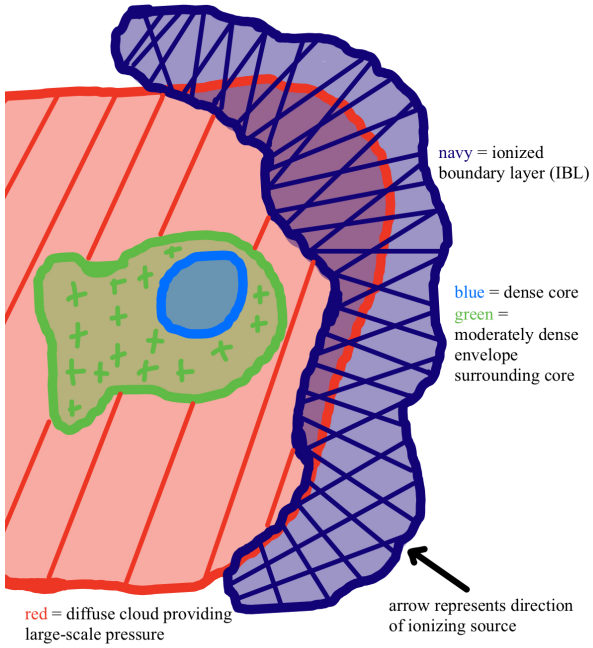

Figure 12. A sample model for bright-rimmed clouds where photoionization triggering is likely.

distributed 12CO emission. This diffuse cloud supports the PDR and ionized boundary layer, and it can be presumed based on previous and current data that this area of the cloud had a photoionization shock propagate through it awhile ago. At the outermost layer of the cloud is the external PDR that, while being heated itself, heats the rest of the BRC and is likely sending pressure waves through the cloud as well. Morgan et al. (2004) found that many clouds in the SFO catalogue are in a shocked or post-shocked state, although this determination was unable to be made explicitly in the case of SFO 14, due to the unclear emission from the embedded star formation within the cloud.

While we are beginning to form a qualitative picture of SFO 14 and star formation in a set of BRCs in the SFO catalog, more observations may be needed to complete the picture. It may be recommended that the CO data be re-observed for SFO 14, as there are a number of dead pixels in the data that, if observed clearly, may be able to provide more clarity as to the cloud's behavior. In order to perform a comprehensive analysis of all the BRCs in the SFO catalogue, the process of creating CO parameter maps and comparing them to the ammonia maps must be replicated for each BRC. Once this process has been repeated for multiple objects, patterns will start to emerge that can lead to refinement of the model. A complete and accurate model to describe star formation in BRCs is key to confirming that said star formation is triggered.

ACKNOWLEDGMENTS

I would like to thank the Green Bank Observatory and the National Radio Astronomy Observatory for selecting me to participate in summer research and Larry for guiding and supporting me along the way.

REFERENCES

Bertoldi, F. 1989, ApJ, 346, 735. doi:10.1086/168055

Lefloch, B. & Lazareff, B. 1994, A&A, 289, 559

Morgan, L. K., Thompson, M. A., Urquhart, J. S., et al. 2004, A&A, 426, 535. doi:10.1051/0004-6361:20040226

Morgan, L. K., Thompson, M. A., Urquhart, J. S., et al. 2008, A&A, 477, 557. doi:10.1051/0004-6361:20078104

Morgan, L. K., Urquhart, J. S., & Thompson, M. A. 2009, MNRAS, 400, 1726. doi:10.1111/j.1365-2966.2009.15585

Morgan, L. K., Figura, C. C., Urquhart, J. S., et al. 2010, MNRAS, 408, 157. doi:10.1111/j.1365-2966.2010.17134

Sugitani, K., Fukui, Y., & Ogura, K. 1991, ApJS, 77, 59. doi:10.1086/191597